

## Placing a small-scale Vertical Axis Wind Turbine on roof-top corner of a building

Farshad Rezaei<sup>1</sup>, Marius Paraschivoiu<sup>2</sup>,

<sup>1,2</sup>Department of Mechanical, Industrial, and Aerospace Engineering, Concordia University, Montreal, Quebec, Canada

<sup>1</sup>[Farshadrezaei585@gmail.com](mailto:Farshadrezaei585@gmail.com)

<sup>2</sup>[Marius.paraschivoiu@concordia.ca](mailto:Marius.paraschivoiu@concordia.ca)

**Abstract**— The current study demonstrates the very high performance of Vertical-Axis Wind Turbine (VAWT) on the roof-top corner of a building using Computational Fluid Dynamics (CFD). A small-scale VAWT with high rotational velocity is validated using the SST  $k-\omega$  turbulence model. It is shown that this turbulence model can predict the flow field around and the performance of the turbine accurately in comparison with experimental results. By locating the turbine on the corner of the building and having the wind at an angle of  $45^\circ$  with respect to the face of the building, it is found that the power coefficient of the turbine increases significantly at higher values of Tip Speed Ratios (TSRs). Nevertheless, it is found that by doubling the Aspect ratio (AR) of the turbine, its performance decreased.

**Keywords-component;** *Vertical Axis wind Turbine- Computational Fluid Dynamics- Roof top- Building- Tip Speed Ratio- Aspect Ratio*

### I. INTRODUCTION

Due to its pollution-free power generation capabilities and worldwide availability of wind resources, wind energy is a promising technology in the electricity generation field. The rising energy demand can be mitigated by installing wind turbines to the maximum extent possible. Wind turbines are divided—based on the axis of rotation—into two main categories; Horizontal Axis Wind Turbine (HAWT) and Vertical Axis Wind Turbine (VAWT). Since VAWTs are slightly less efficient than HAWTs, the HAWT is the primary type of wind turbine in use today and has received a great deal of attention in both the research and industrial sectors [1] [2] [3]. While HAWTs requires a uniform airflow into their rotor surface, which retains the produced torque constantly, VAWTs can perform well in more complex winds due to capture the wind from all the directions.

Consequently, they have induced fluctuation torque [4]. Nevertheless, VAWTs have such principal advantages as being Omni-directional, having low installation and maintenance cost, low center of gravity, and low scalability, making them suitable to use in specific regions such as urban areas and off-shore. Mollerstrom et al. did a historical review of VAWTs

[5]. Among different VAWTs, the Darrieus type is considered one of the most attractive VAWTs due to the low visual impact and acoustic emissions and their appropriate response to a turbulent oncoming flow. To increase the power production of VAWTs, many researchers have worked on blade aerodynamics optimization such as chord and camber length, pitch angle, and thickness of the trailing edge [6] [7] [8] [9].

Wind energy potential is high on roof-tops of high-rise buildings. Urban wind energy is attractive because it can provide energy close to demand and reduce the cost of power distribution. Tasneem et al. summarized the present status of wind farm technologies in urban areas in a review paper [10]. They concluded that further wind mapping research and turbine design improvements are required for the urban wind farm to be a reliable and feasible option for decentralized power generation. The potential mounting sites of wind turbines by considering the details of the local urban topography is studied numerically by Yang et al. [11]. They showed that increasing the hub height and installing micro-turbines on the windward side of the building have positive effects on higher power production. Balduzzi et al. characterized the flow field above the roof-top of buildings with different geometries numerically [12]. They used other oncoming wind profiles and calculated their specific velocity modulus and direction on the roof-top of each building. They reported that the attained capacity of VAWT installed on the roof-top of a building higher than surrounding buildings could be increased up to 70%.

To improve the performance of the VAWTs, efficient design and optimized location of the turbines, especially on roof-mounted buildings, are fundamental. The effects of vertical wind, wind direction, and turbulence intensity on the power output of a small VAWT in an environment were investigated by Lee et al. [13]. Their results indicate that more than 90% of the power could be generated if the vertical angle was less than or equal to  $45^\circ$ . Bashirzadeh Tabrizi et al. modeled wind flows over the roof of a building by a CFD code [14]. Abohela et al. used numerical simulations to find the effects of different roof shapes, building height, and wind directions [15]. They illustrated that high-rise buildings are better choices while the turbine is installed near the edge of the building. To find an evaluation tool for wind energy resources

by using small wind turbines on the roof-top of a building, they evaluated the possibility of combining with a wind atlas software. Their results showed that the building height, wind direction, and turbine installation height affect the wind turbine performance. Based on relevant installation guidelines, small wind turbines are usually used in complex environments like roof-tops of high buildings rather than open terrain sites [16]. To investigate wind turbine performance and the synergy between them and the urban environments, Dilimulati et al. reviewed urban wind energy by examining different types of wind turbines [17]. They showed that although airflow's velocity and density increase in urban areas, there is a very turbulent flow due to the increased ground roughness and unpredictable airflow direction. This turbulent flow reduces the efficiency of the HAWTs. Therefore, using VAWTs is recommended in urban areas [18].

Moreover, an field experimental analysis was performed by Pagnini et al. to compare HAWT and VAWT in the same urban environment [19]. They showed that solid winds caused much less damage to VAWTs than HAWTs. Therefore, VAWTs could be operated at higher wind velocities. Moreover, they showed high production losses for higher wind velocity than 6-7 m/s, while the ambient turbulence could not be considered the main reason for such reduction. Also, Aslam Bhutta et al. showed that in places with complex flow patterns such as roof-tops of building in urban built environments, VAWTs have better performance than HAWTs [20]. Since Darrieus types of the VAWTs produce low acoustic emissions and have an appropriate efficiency, they are widely used in roof-top installation [12]. Zabarjad Shiraz et al. analyzed the energy production of roof-mounted Darrieus wind turbine in a city by using both CFD and meteorological data related to that city [21]. They provided the energy yield of the turbine located at each of the four corners of a building for different urban density environments. Their simulation showed a reduction in energy production in high-density urban environments because of local wind behavior.

It is still challenging to obtain reliable and consistent data about the efficiency of wind turbines in urban environments. Some researchers investigated wind turbines in the urban built environment from the economic viewpoint by considering parameters such as available locations, prevailing wind speeds, and storage systems [22]. Although the energy potential of the urban environment is high, using wind turbines in the urban built environment is still at the early stages of their development; therefore, more research is necessary. This study focuses on two objects; first, a small-scale Darrieus wind turbine, an H-type with high rotational velocity, is studied using the SST  $k-\omega$  turbulence model. Second, the performance of the turbine on a building with a height of 30.48 m (100 ft) is studied by considering its location based on the suggestion of [13] [15] [21]. This work starts by explaining the numerical setup. Then, the turbine's performance is analyzed and

compared with other published results. In this section, the performance of the SST  $k-\omega$  turbulence model is investigated. Then, the performance of the turbine on the building is evaluated.

## II. NUMERICAL SETUP

### A. Configuration and numerical modeling

In this study, a small-scale two-bladed H-type of VAWT is studied. Table 1 shows the geometrical data of the turbine, which are used in the current study. To model the turbulent flow around the VAWT, URANS equations are complemented with the SST  $k-\omega$  turbulence model as suggested by [23] [24] [25] [26]. Therefore, in the current research, the SST  $k-\omega$  model is used. STAR CCM+, a commercial CFD solver, is used to solve the equations of motion and capture all flow field features. An implicit unsteady segregated flow method is employed. The SIMPLE algorithm (Semi-Implicit Method for Pressure Linked Equations) is employed to couple the pressure-velocity equations. Also, a second-order upwind scheme is used for the convection terms. This study is focused on the turbine rotating with high rotational velocity. This velocity is expressed in a non-dimensional number named Tip Speed Ratio (TSR), calculated as:

$$TSR=R\omega/U_\infty \quad (1)$$

where  $R$  is the turbine radius and  $\omega$  is the angular velocity of the turbine. The available power from the wind turbine is given by:

$$P_{wind}=0.5\rho A_S U_\infty^3 \quad (2)$$

where  $\rho$  is the air density,  $U_\infty$  is the free stream velocity, and  $A_S$  is the swept area equal to the turbine diameter multiplied by the blade span. The power coefficient is a non-dimensional parameter defined as the ratio of the power extracted from the turbine to the available capacity (2).

$$C_P=P_{turbine}/P_{wind} \quad (3)$$

To have a moving boundary 3-D simulation, the computational domain needs to be partitioned into the rotor and wind tunnel domains. The rotor domain, which is rotating, includes the blades. This rotating domain is encapsulated inside the wind tunnel domain, as illustrated in Fig. 1.

TABLE I. GEOMETRICAL DATA OF THE VAWT

Turbine diameter, D	1 m
Blade span, L	1 m
Blade chord length, c	0.06 m
Airfoil section	NACA 0018
Number of blades	2
Solidity, $\sigma$	0.12
Aspect ratio, L/D	1

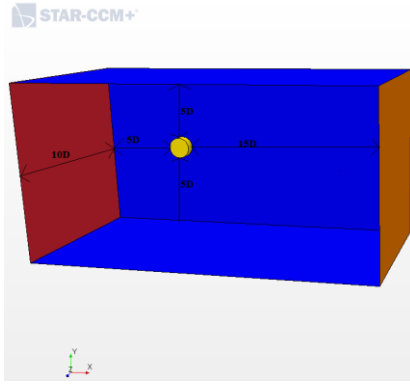


Figure 1. Computational domain

To avoid interferences caused by the boundaries, the dimensions of both rotor and wind tunnel domains were carefully considered [23] [27], as depicted in Fig.1. The long-distance behind the rotor and the end of the computational domain is necessary to provide enough space for the wake generation. Velocity inlet and pressure outlet are considered at the inlet and outlet boundaries, respectively. The wind velocity is constant, equal to  $9.3 \text{ m/s}$ , while rotational speed is changed to have different values of TSRs. The pressure at the outlet is considered a value of  $0 \text{ Pa}$ , which shows the air pressure at the exit of the wind tunnel domain. Symmetry boundary condition is employed for the other four boundaries of the wind tunnel domain. Boolean and Subtract operations are used to remove a cylindrical shape representing the rotor section from the wind tunnel domain. The rotor section and the wind tunnel section were meshed separately. The mesh size at the rotor's surface is kept equal with the wind tunnel domain's surface, where a cylindrical shape similar to the rotor is subtracted. This matching of the two sections will help complete mapping between the rotor and the wind tunnel domain. The interface boundary condition is employed between the two sections to ensure the fluid flow between them.

### B. Mesh study

Mesh quality plays an essential role in the CFD results. Four different meshes are used in this study to ensure the results are independent of the grid. A grid-independent solution is achieved when there is a negligible difference between the average power coefficients of two different meshes. Moreover, the results are compared with a numerical simulation [27] and the classical double-multiple stream-tube (DMST) method [28]. In the DMST model, the calculations for the upstream and downstream half- revolutions are performed separately. More information on this model can be found in [29]. Comparison among the four forgoing meshes is made at a rotational velocity of  $83.7 \text{ rad/s}$  and a TSR of 4.5. Table 2 shows the information associated with the four different meshes. During the grid generation, the first layer close to the solid surface needs more attention. For that layer, the value of the  $Y^+$  should be around 1.  $Y^+$  is a non-dimensional parameter defined based on wall shear stress. The value of  $Y^+$  for both Mesh 1 and Mesh 2 are less than 1. So, by reducing the blade surface size, it is found that the value of  $C_p$  increased. Since the value of  $Y^+$  is far less

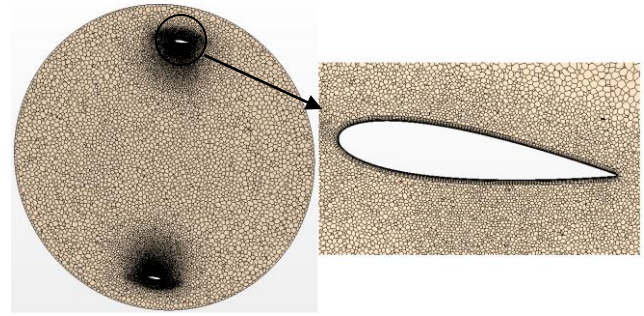


Figure 2. The mesh in a section of the rotor (left), prism layer mesh around the airfoil

than 1, to reduce the computational cost, the first layer thickness increases while the blade surface size decreases in Mesh 3. Moreover, the blade surface size varied from 0.0004 to 0.00075 meters; in a way that the size of both leading and trailing edges are smaller than the middle section of the airfoil. Although the values of  $Y^+$  are close to 1 for Mesh 3, it is found that  $Y^+$  is increased to values of more than 1 for high angles of attack. For Mesh 4, both the values of first layer thickness and the blade surface size are reduced slightly; it is found that the value of  $C_p$  is not such changed. For this mesh, the values of  $Y^+$  are close to 1 for all angles of attack. Fig. 3 shows the values of  $C_p$  for different meshes and compares it with another similar simulation [27] and the DMST method [28]. Lam and Peng [27] used both Detached Eddy Simulation (DES) and Transition Shear Stress Transport (SST) method for their simulation. Figure 2 shows a good agreement with the current simulation, using SST  $k-\omega$  method, and the results from the SST method.

TABLE II. DATA OF FOUR DIFFERENT MESHES AND THEIR  $C_p$

Mesh Name	First layer Thickness (m)	Blade surface size (m)	$C_p$
Mesh 1	$5.82 \text{ e-}6$	0.00075	0.2202
Mesh 2	$5.82 \text{ e-}6$	0.00062	0.2412
Mesh 3	$1.428 \text{ e-}5$	0.0004 to 0.00075	0.2652
Mesh 4	$8.8 \text{ e-}6$	0.00036 to 0.00069	0.2720

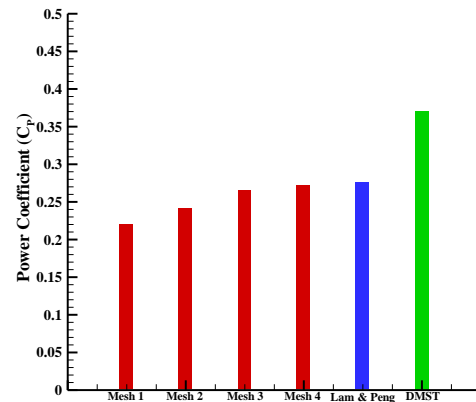


Figure 3. Results at TSR=4.5 for different meshes and compare with another numerical simulation [27] and DMST method [28]

### C. Temporal convergence

A detailed study is performed for the time step [30] [31]. The time steps that researchers frequently use to simulate VAWTs varied from  $0.2^\circ$  to  $1.2^\circ$  rotation of blades per time step. The time step that Lam and Peng [27] used was  $1.04 \times 10^{-4}$  second, equivalent to  $0.5^\circ$  rotation of blades per time step. In this study, two different time steps are used for the TSR value of 4.5, which are  $0.0001$  s and  $0.00005$  s, equal to  $0.48^\circ$  and  $0.24^\circ$  rotation of the blades per time step, respectively. Fig. 4 shows that both time steps predict the same values as they become stable. Therefore, to keep the computational cost low, the time step  $0.0001$  s is selected for this study. Fig. 4 shows that the simulations are converged after 15 revolutions.

### D. Validation with experimental data

Fig. 5 shows a comparison between Particle Image Velocimetry (PIV) test results [32] and current simulations for more validation. Also, the results from another numerical simulation that used Detached Eddy Simulation (DES) are compared. The stream-wise wake velocity at a distance equal to one diameter of the rotor in the wake region is shown in Fig. 5. This figure shows that there is an encouraging overall matching. At the region of  $Y/D < 0$ , the magnitudes of the velocity deficit are excellently captured by the current simulation. At the  $Y/D > 0$ , the CFD simulation could not capture the strong wake expansions very well, which appeared in the PIV test. An important reason for that is related to the neglected four struts and connections between blades and struts in the numerical simulation; while they were used in experimental tests. Those struts and linkages have blockage effects on the air flows [27]. Consequently, by accelerating the airflows near the struts, the swirling momentum increases and strengthens the windward transport of the wake.

Fig. 6 shows the values of  $C_p$  for different values of TSR. It shows that current simulation and DMST results have the same trend. Both of them calculate the maximum  $C_p$  at the TSR of 4. Moreover, they predicted the close values of  $C_p$  at the TSR of 5. The differences between the values of  $C_p$  in CFD simulation and the DMST model are attributed to the fact that the DMST model cannot calculate the flow motions along the span and the vertical motions at the tips.

Consequently, it predicted higher values of  $C_p$ . The discrepancies between the current simulation and the other CFD results from the literature [27] at small TSR values may be related to the mesh structures. As discussed in the previous section, mesh structures are sensitive to the stall condition since there is a strong stall behavior at small values of TSR.

### III. PLACING THE TURBINE ON THE ROOF-TOP OF A BUILDING

The computational domain for the building study is shown in Fig. 7. Lee et al. suggested that the maximum  $C_p$  could be achieved by locating the VAWT on the corner of the building with an angle of  $45^\circ$  [13]. To have this angle, instead of having the angle for the velocity inlet, the building has the angle of  $45^\circ$  regarding the inlet, as shown in Fig. 7. Zabarjad Shiraz et al. suggested locating the turbine at the corners of the building [21]. In this study, the turbine is located on a building with an angle of  $45^\circ$  with the inlet velocity and on a corner close to the

inlet section. The turbine is located at a  $2D$  height from the building roof. The computational domain size is based on the suggestion of Weerasuriya's study [33].

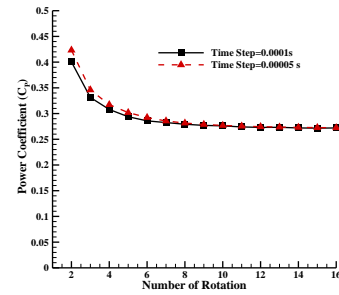


Figure 4.  $C_p$  vs. number of rotations for two different time steps

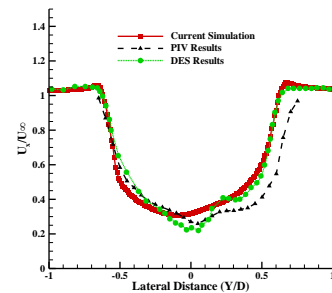


Figure 5. Comparisons of velocities between current simulation, PIV tests [32], and another numerical simulation [27] at wake region equal to  $1.0D$

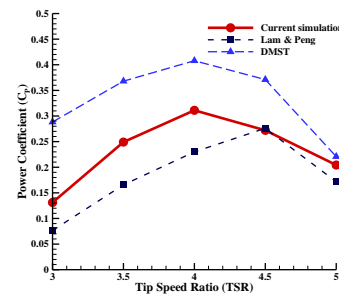


Figure 6. Comparisons of  $C_p$  for different TSRs between current simulation, DMST method [28], and another numerical solution [27]

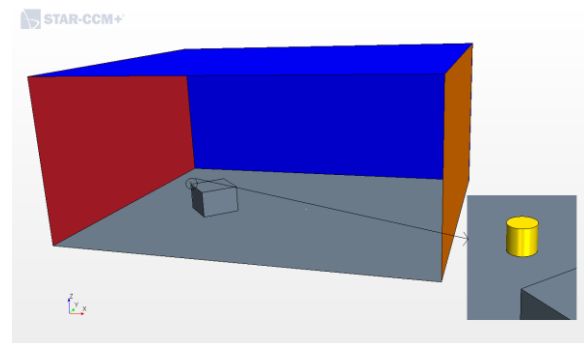


Figure 7. Computational domain for the building

To measure the performance of VAWT on the roof-top of a building, a building with a height of 30.48 m (100 ft) is considered. Six simulations are done for different TSRs ranging from 3 to 5.5, with the same CFD model, mesh, and time step information used in the previous section. As wind turbines operate in the atmospheric boundary layer, in each of the test cases, the inlet boundary is defined with a wind velocity profile to account for the effects of the atmospheric boundary layer, where the wind velocity is a function of height, defined as follows:

$$V_z = V_{mid}(Z/H_t)^{0.31} \quad (4)$$

where  $V_{mid}$  is the wind velocity at the middle of the turbine,  $Z$  is the height from the ground, and  $H_t$  is the height from the ground to the center of the turbine. This velocity profile is shown in Fig. 8. To eliminate the reverse flow effects, the inlet distance from the upstream edge of the building and the outlet boundary behind the downstream edge of the building are considered  $3H$  and  $10H$ , respectively. The power coefficient achieved by the turbine is shown in Fig. 9, compared with the unperturbed case, reviewed in the previous section. It shows that for the values of TSR which are smaller than 4, the  $C_p$  are decreased on the building. In small values of TSR, since there is a strong stall, the Atmospheric Boundary Layer (ABL) affects the turbine performance. So, the turbine produces small power. Moreover, it can be seen that the differences between the building case and the unperturbed case are almost the same at both TSRs of 3 and 3.5. This shows that the building decreases the  $C_p$  of the turbine uniformly at smaller TSRs than the TSR of 4. Nevertheless, for TSR of 4 and higher, the  $C_p$  is increased. It is shown that for TSR 4.5 and 5, the values of  $C_p$  are increased significantly. Fig. 9 shows that between TSR of 4 and 5, the power increased by the same rate. Therefore, putting the turbine on the building has remarkable effects. These results are close to [13], which predicted 90% of the increase in power by putting the turbine on the roof-top of a building. Also, it is shown at TSR 5.5 that  $C_p$ 's value decreased than its values at TSR 5. At higher values of TSR, blades have experienced smaller flow separations, mainly when the rotor rotates faster. As a result, they can produce higher power. Table 3 shows the result of  $C_p$  for a bigger turbine with a double Aspect Ratio ( $AR=2$ ) at TSR 5. For this case, the ABL is changed, so the turbine works with the same TSR 5— $V_{mid}$  senses the turbine at a higher height. It shows that by doubling the AR, the  $C_p$  decreased. Since the atmospheric is changed for AR of 2, the higher length of the turbine, equal to the case of AR of 1, sense smaller wind velocity than the value of 9.3 m/s. In other words, half of the turbine sense smaller values of TSR. Because of that, the value of  $C_p$  decreased. Fig. 10 shows the streamlines at the edge of the roof of the building and behind the turbine. It shows that the 2D distance between the turbine and the roof is enough to locate the turbine since the effects of the roof on the flow field are at their minimum. Moreover, streamlines behind the turbine show that more studies are necessary to find the wake characteristics of the flow field behind the turbine on the roof of the building.

#### IV. CONCLUSION

A small-scale VAWT with high rotation velocity is modeled by using SST  $k-\omega$  turbulence model at different TSR

values. Compared with experimental results, it is found that this turbulence model could predict the flow field features around the turbine with high accuracy. Power coefficient of for different values of TSR calculated; the maximum power coefficient found at TSR of 4, in agreement with DMST model. By placing the turbine on a roof-top of building with the height of 30.48 m (100 ft), it is found that the power coefficient decreased at TSR values less than 4; while its value increased for TSR of 4 and more. The best power on the building is achieved by TSR of 5, while its power without building is not significant. The turbine performance over the roof-top of a building at its maximum TSR, which is TSR of 5, is analyzed for a turbine with double AR. It is found that the performance of the turbine decreased at higher AR.

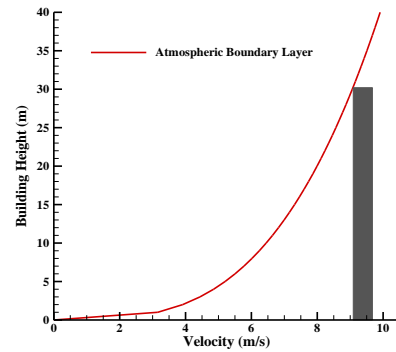


Figure 8. The schematic of the atmospheric boundary layer over a building

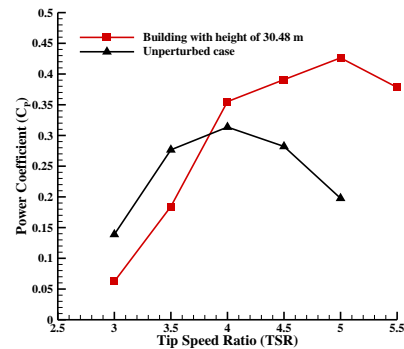


Figure 9. Power coefficient for the unperturbed case and the building case

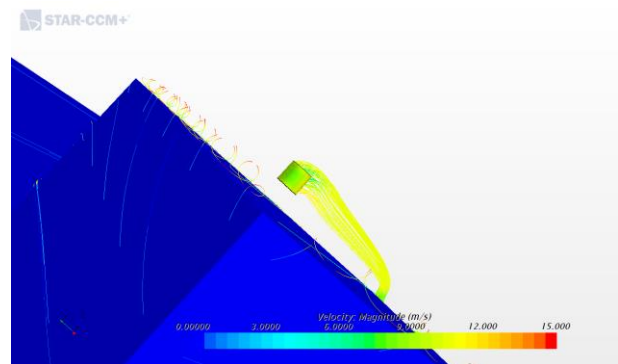


Figure 10. Streamlines over the building and behind the turbine

TABLE III. POWER COEFFICIENT FOR DIFFERENT TURBINE'S AR OVER THE BUILDING

Turbine's AR	$C_p$
1	0.426
2	0.385

## V. REFERENCES

- [1] A. M. AbdelSalam and V. Ramalingam, "Wake prediction of horizontal-axis wind turbine using full-rotor modeling," *J. Wind Eng. Ind. Aerodyn.*, vol. 124, pp. 7–19, 2014, doi: 10.1016/j.jweia.2013.11.005.
- [2] M. Bastankhah and F. Porté-Agel, "A new analytical model for wind-turbine wakes," *Renew. Energy*, vol. 70, pp. 116–123, 2014, doi: 10.1016/j.renene.2014.01.002.
- [3] C. J. Bai and W. C. Wang, "Review of computational and experimental approaches to analysis of aerodynamic performance in horizontal-axis wind turbines (HAWTs)," *Renew. Sustain. Energy Rev.*, vol. 63, pp. 506–519, 2016, doi: 10.1016/j.rser.2016.05.078.
- [4] W. Tjiu, T. Marnoto, S. Mat, M. H. Ruslan, and K. Sopian, "Darrieus vertical axis wind turbine for power generation II: Challenges in HAWT and the opportunity of multi-megawatt Darrieus VAWT development," *Renew. Energy*, vol. 75, pp. 560–571, 2015, doi: 10.1016/j.renene.2014.10.039.
- [5] E. Möllerström, P. Gipe, J. Beurskens, and F. Ottermo, "A historical review of vertical axis wind turbines rated 100 kW and above," *Renew. Sustain. Energy Rev.*, vol. 105, no. January, pp. 1–13, 2019, doi: 10.1016/j.rser.2018.12.022.
- [6] M. Elkhoury, T. Kiwata, and E. Aoun, "Experimental and numerical investigation of a three-dimensional vertical-axis wind turbine with variable-pitch," *J. Wind Eng. Ind. Aerodyn.*, vol. 139, pp. 111–123, 2015, doi: 10.1016/j.jweia.2015.01.004.
- [7] J. Chen, L. Chen, H. Xu, H. Yang, C. Ye, and D. Liu, "Performance improvement of a vertical axis wind turbine by comprehensive assessment of an airfoil family," *Energy*, vol. 114, pp. 318–331, 2016, doi: 10.1016/j.energy.2016.08.005.
- [8] X. Zhang, Z. Li, X. Yu, and W. Li, "Aerodynamic Performance of Trailing-Edge Modification of H-Type VAWT Blade Considering Camber Effect," *Int. J. Aeronaut. Sp. Sci.*, 2019, doi: 10.1007/s42405-019-00241-x.
- [9] T. Zhang, Z. Wang, W. Huang, D. Ingham, L. Ma, and M. Pourkashanian, "A numerical study on choosing the best configuration of the blade for vertical axis wind turbines," *J. Wind Eng. Ind. Aerodyn.*, vol. 201, no. January, 2020, doi: 10.1016/j.jweia.2020.104162.
- [10] Z. Tasneem *et al.*, "An analytical review on the evaluation of wind resource and wind turbine for urban application: Prospect and challenges," *Dev. Built Environ.*, vol. 4, no. October, p. 100033, 2020, doi: 10.1016/j.dibe.2020.100033.
- [11] A. S. Yang, Y. M. Su, C. Y. Wen, Y. H. Juan, W. S. Wang, and C. H. Cheng, "Estimation of wind power generation in dense urban area," *Appl. Energy*, vol. 171, pp. 213–230, 2016, doi: 10.1016/j.apenergy.2016.03.007.
- [12] F. Balduzzi, A. Bianchini, E. A. Carnevale, L. Ferrari, and S. Magnani, "Feasibility analysis of a Darrieus vertical-axis wind turbine installation in the roof-top of a building," *Appl. Energy*, vol. 97, pp. 921–929, 2012, doi: 10.1016/j.apenergy.2011.12.008.
- [13] K. Y. Lee, S. H. Tsao, C. W. Tzeng, and H. J. Lin, "Influence of the vertical wind and wind direction on the power output of a small vertical-axis wind turbine installed on the roof-top of a building," *Appl. Energy*, vol. 209, no. May, pp. 383–391, 2018, doi: 10.1016/j.apenergy.2017.08.185.
- [14] A. B. Tabrizi, J. Whale, T. Lyons, and T. Urmee, "Performance and safety of roof-top wind turbines: Use of CFD to gain insight into inflow conditions," *Renew. Energy*, vol. 67, pp. 242–251, 2014, doi: 10.1016/j.renene.2013.11.033.
- [15] I. Abohela, N. Hamza, and S. Dudek, "Effect of roof shape, wind direction, building height and urban configuration on the energy yield and positioning of roof mounted wind turbines," *Renew. Energy*, vol. 50, pp. 1106–1118, 2013, doi: 10.1016/j.renene.2012.08.068.
- [16] A. B. Tabrizi, J. Whale, T. Lyons, and T. Urmee, "Roof-top wind monitoring campaigns for small wind turbine applications: Effect of sampling rate and averaging period," *Renew. Energy*, vol. 77, pp. 320–330, 2015, doi: 10.1016/j.renene.2014.12.037.
- [17] A. Dilimulati, T. Stathopoulos, and M. Paraschivoiu, "Wind turbine designs for urban applications: A case study of shrouded diffuser casing for turbines," *J. Wind Eng. Ind. Aerodyn.*, vol. 175, no. February, pp. 179–192, 2018, doi: 10.1016/j.jweia.2018.01.003.
- [18] J. Cace *et al.*, "Urban wind turbines - guidelines for small wind turbines in the built environment," pp. 1–41, 2007.
- [19] L. C. Pagnini, M. Burlando, and M. P. Repetto, "Experimental power curve of small-size wind turbines in turbulent urban environment," *Appl. Energy*, vol. 154, pp. 112–121, 2015, doi: 10.1016/j.apenergy.2015.04.117.
- [20] M. M. Aslam Bhutta, N. Hayat, A. U. Farooq, Z. Ali, S. R. Jamil, and Z. Hussain, "Vertical axis wind turbine - A review of various configurations and design techniques," *Renew. Sustain. Energy Rev.*, vol. 16, no. 4, pp. 1926–1939, 2012, doi: 10.1016/j.rser.2011.12.004.
- [21] M. Zabarjad Shiraz, A. Dilimulati, and M. Paraschivoiu, "Wind power potential assessment of roof mounted wind turbines in cities," *Sustain. Cities Soc.*, vol. 53, no. May, 2019, 2020, doi: 10.1016/j.scs.2019.101905.
- [22] B. Grieser, Y. Sunak, and R. Madlener, "Economics of small wind turbines in urban settings: An empirical investigation for Germany," *Renew. Energy*, vol. 78, no. October, pp. 334–350, 2015, doi: 10.1016/j.renene.2015.01.008.
- [23] B. Belabes and M. Paraschivoiu, "Numerical study of the effect of turbulence intensity on VAWT performance," *Energy*, vol. 233, p. 121139, 2021, doi: 10.1016/j.energy.2021.121139.
- [24] F. Balduzzi, J. Drofelnik, A. Bianchini, G. Ferrara, L. Ferrari, and M. S. Campobasso, "Darrieus wind turbine blade unsteady aerodynamics: a three-dimensional Navier-Stokes CFD assessment," *Energy*, vol. 128, pp. 550–563, 2017, doi: 10.1016/j.energy.2017.04.017.
- [25] Q. Li *et al.*, "Wind tunnel and numerical study of a straight-bladed vertical axis wind turbine in three-dimensional analysis (Part I: For predicting aerodynamic loads and performance)," *Energy*, vol. 106, pp. 443–452, 2016, doi: 10.1016/j.energy.2016.03.089.
- [26] M. Raciti Castelli, A. Dal Monte, M. Quaresimin, and E. Benini, "Numerical evaluation of aerodynamic and inertial contributions to Darrieus wind turbine blade deformation," *Renew. Energy*, vol. 51, pp. 101–112, 2013, doi: 10.1016/j.renene.2012.07.025.
- [27] H. F. Lam and H. Y. Peng, "Study of wake characteristics of a vertical axis wind turbine by two- and three-dimensional computational fluid dynamics simulations," *Renew. Energy*, vol. 90, pp. 386–398, 2016, doi: 10.1016/j.renene.2016.01.011.
- [28] H. Beri and Y. Yao, "Double Multiple Streamtube Model and Numerical Analysis of Vertical Axis Wind Turbine," *Energy Power Eng.*, vol. 03, no. 03, pp. 262–270, 2011, doi: 10.4236/epe.2011.33033.
- [29] I. Paraschivoiu, "Double-multiple streamtube model for studying vertical-axis wind turbines," *J. Propuls. Power*, vol. 4, no. 4, pp. 370–377, 1988, doi: 10.2514/3.23076.
- [30] A. Rezaeiha, I. Kalkman, and B. Blocken, "CFD simulation of a vertical axis wind turbine operating at a moderate tip speed ratio: Guidelines for minimum domain size and azimuthal increment," *Renew. Energy*, vol. 107, pp. 373–385, 2017, doi: 10.1016/j.renene.2017.02.006.
- [31] A. Rezaeiha, H. Montazeri, and B. Blocken, "Towards accurate CFD simulations of vertical axis wind turbines at different tip speed ratios and solidities: Guidelines for azimuthal increment, domain size and convergence," *Energy Convers. Manag.*, vol. 156, no. October, pp. 301–316, 2018, doi: 10.1016/j.enconman.2017.11.026.
- [32] G. Tescione, D. Ragni, C. He, C. J. Simão Ferreira, and G. J. W. van Bussel, "Near wake flow analysis of a vertical axis wind turbine by stereoscopic particle image velocimetry," *Renew. Energy*, vol. 70, pp. 47–61, 2014, doi: 10.1016/j.renene.2014.02.042.
- [33] A. U. Weerasuriya, "Computational Fluid Dynamic (CFD) simulation of flow around tall buildings," *Eng. J. Inst. Eng. Sri Lanka*, vol. 46, no. 3, p. 43, 2013, doi: 10.4038/engineer.v46i3.6784.